energies

MDPI

Article

Modelling and Measurement of a Moving Magnet Linear Motor for Linear Compressor

Xinwen Chen [1], Hanying Jiang [2,*], Zhaohua Li [2] and Kun Liang [1,2,*]

[1] Department of Mechanical Engineering, Yangzhou University, Yangzhou 225012, China; xwchen0513@163.com
[2] Department of Engineering and Design, University of Sussex, Brighton BN1 9QT, UK; zl282@sussex.ac.uk
* Correspondence: hj203@sussex.ac.uk (H.J.); kun.liang@sussex.ac.uk (K.L.)

Received: 19 June 2020; Accepted: 3 August 2020; Published: 4 August 2020

Abstract: For the purpose of efficiency improvement, a linear motor that performs a linear reciprocating motion can be employed to directly drive the piston in a reciprocating refrigeration compressor without crankshaft mechanism. This also facilitates the modulation of cooling capacity as the stroke and frequency can be readily varied in response to heat load. A novel design of moving magnet linear motor for linear compressor was analyzed in the paper. A finite element analysis (FEA) model was built to simulate the characteristics of the linear motor. Current and displacement signals were measured from a test rig and were defined in the transient FEA model. Transient motor force was simulated with the FEA model and good agreements are shown between the results from the FEA model and interpolated shaft force from static force measurements. Major Losses, such as copper loss and core loss were also computed. Motor efficiency decreased from 0.88 to 0.83 as stroke increased from 9 mm to 12 mm, while the pressure ratio remained unchanged. Comparisons were made between the present moving magnet linear motor and moving coil linear motors. Generally, the moving magnet linear motor demonstrates higher efficiency than moving coil motors, which have significantly higher copper loss. The present moving magnet design with simple structure could be further optimized to improve motor efficiency.

Keywords: linear motor; moving magnet; FEA; motor loss; motor efficiency; moving coil

1. Introduction

Refrigeration systems consume around 17% of the electricity in the world, where more than 1.5 billion household refrigerators are in use currently [1]. Linear motor has been employed for linear compressors in refrigeration systems to provide reciprocating motion. Linear motor shows good linearity and eliminates motion conversion mechanisms that transfer rotary motion into linear motion. The elimination of these mechanical components leads to improvement in reliability and dynamic performance and also decreasing mechanical friction loss [2,3]. A critical feature of a linear compressor directly driven by a linear motor is that the stroke can be readily adjusted, whereas the stroke is fixed in a conventional reciprocating compressor. This offers a simple cooling capacity modulation approach according to the heat load, leading to significantly higher seasonal energy efficiency without any on-off cycling losses.

The overview of the linear motor topologies, applications, and design methodologies was reported by Boldea and Nasra [4]. Different linear motor topologies and technologies can be adopted for linear compressor applications. Most widely used linear motors are linear permanent magnet motors, linear induction motors, and linear switched reluctance motors. Due to their significantly greater efficiency and larger power density, linear permanent magnet motors are considered as the most appropriated ones for linear compressor applications.

Existing permanent magnet linear motors are categorized as: moving coil, moving magnet, and moving iron only as shown in Figure 1. In general, each type of permanent magnet linear motor has its own pros and cons, depending on their practical applications. Moving coil type linear motors have a simple structure, but with wires wound around the moving part, the wiring is not firm and the generated heat is difficult to dissipate. Moving iron type linear motors are robust and cost-effective, but their low efficiency is the major weakness [5]. Recently, investigations have been carried out for moving magnet type linear motors, and various topologies for different applications have been reported [6–12]. In industry, companies have produced some moving magnet linear motors for their application into linear compressors employed in domestic refrigerators [6–8]. The energy-saving effect is significant, compared with conventional systems using rotatory motors and crank-driven mechanism [13].

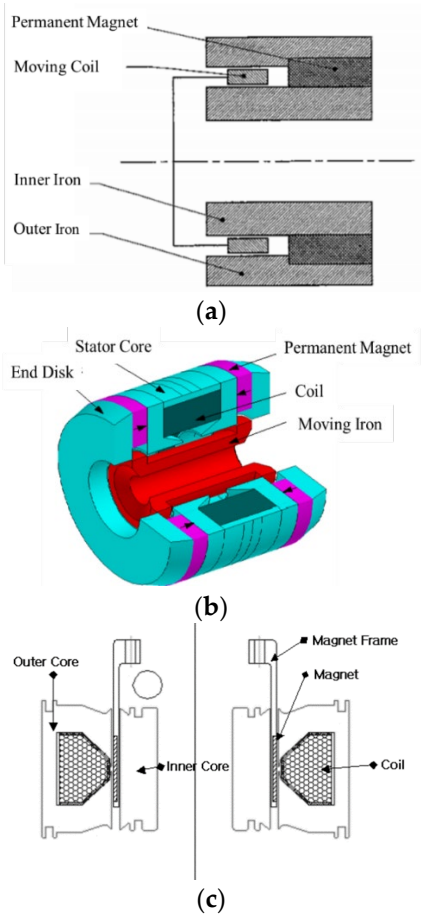

Figure 1. Examples of three types of linear motors: (**a**) moving coil [14] (**b**) moving iron [15] (**c**) moving magnet [16].

To analyze the performances and electromagnetic characteristics of linear motors, a precise knowledge of the distribution of magnetic field is needed. Numerical and analytical methods can be used for the evaluation of magnetic field distribution. Finite Element Analysis (FEA), as a numerical solution, presents the advantage of considering the nonlinear magnetic saturation of cores and the real geometry of the motor design. By solving the governing equations issued from Maxwell's equations, the magnetic field can be evaluated [17,18]. Static shaft forces for various armature positions of moving magnet linear motor were calculated using FEA [19,20]. Li et al. compared some key performance indexes between a novel moving iron and a moving magnet linear motor [21]. FEA has been employed to optimize the design of linear motors. A tubular moving-magnet linear magnet motor was optimized by Abdalla et al. to improve efficiency and reduce losses [22]. The application of FEA also includes

quantification of eddy current loss in linear permanent magnet motor as presented by Ko et al. [23] and Abdalla et al. [24].

This paper analysed a novel 100 W moving magnet linear motor (shown in Figure 2) for linear compressor. A FEA model was built to study the transient motor force and losses. The presented linear motor consists of three moving magnets and four laminated cores with coils wired around as shown in Figure 1. The maximum stroke is 13 mm and the maximum motor force is 90 N. The simulated transient motor force was compared with the interpolation results based on the static measurements. Core loss, eddy current loss and copper loss were analysed. Motor efficiency was calculated and compared with a moving coil linear motor with comparable dimensions. Section 2 shows the FEA model. The experimental setup was introduced in Section 3. In Section 4, flux density, transient motor force from simulation and measurements, motor losses, and motor efficiency were presented. The novel moving magnet linear motor was compared with other moving coil designs and other moving magnet designs respectively in Sections 5 and 6.

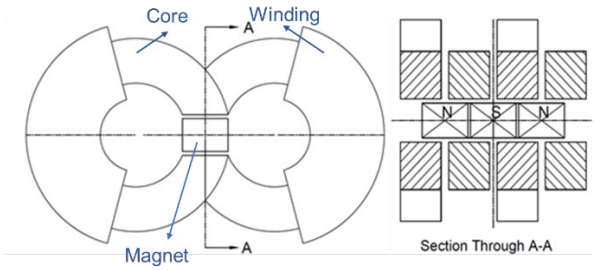

Figure 2. The configuration of the moving magnet linear motor.

2. FEA Model

A three-dimensional (3D) FEA model of the moving magnet linear motor was built in ANSYS Maxwell. In a time-domain transient solution, the instantaneous magnetic field at each time step was solved step by step. In the FEA model, boundary conditions, motor geometry, and all materials properties were defined. Faraday's Law of induction, Gauss's Law for magnetism, Ampere's Law, and Gauss's Law for electricity were included in the Maxwell's equations. Low-frequency forms of Maxwell's equations are employed in ANSYS Maxwell 3D Transient Solver [25]:

$$\nabla \times \frac{1}{\sigma}(\nabla \times H) + \frac{\partial B}{\partial t} = 0 \tag{1}$$

$$\nabla \cdot B = 0 \tag{2}$$

$$-\nabla \cdot \left(\varepsilon \nabla \frac{\partial \Phi}{\partial t}\right) - \nabla \cdot (\sigma \nabla \Phi) = 0 \tag{3}$$

where B is the magnetic flux density, H is the magnetic field strength, Φ is the magnetic flux, σ and ε are the conductivity and permittivity of the material, respectively.

To obtain a closed system, the constitutive relations describing the macroscopic properties of the medium are also included. The electric and magnetic flux density D, B are related to field intensities E, H via the constitutive relations. In magneto-static solver, Maxwell adopts an adaptive iterative process to refine the mesh until required accuracy is met or maximum number of passes is reached. However, transient solver is not capable of improving initial mesh automatically. Figure 3 shows the FEA model of the moving magnet linear motor. More details about the design of the linear motor can be found in the previous study [19]. Current from measurement was applied to each winding, and measured displacement was also defined in the motion setup to include translational motion effects. The nonlinear residual error for the transient solver was set to be 0.001.

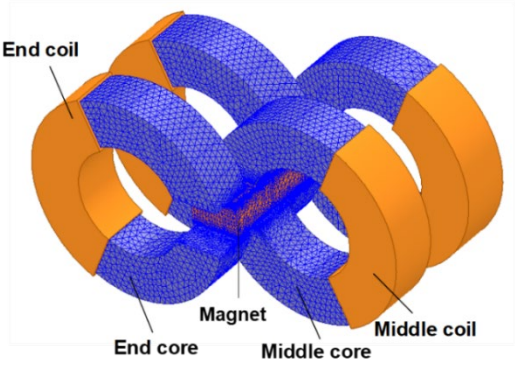

Figure 3. The FEA model of the moving magnet linear motor.

3. Experimental Setup

Experiments were performed in the test rig that was adapted from the previous work [13]. The linear compressor is composed of a piston-cylinder assembly, a linear motor, and a suspension system using flexure spring. The schematic of the test rig using the linear motor is shown in Figure 4. The refrigeration system consists of a linear compressor driven by the moving magnet linear motor, an expansion valve, an evaporator, and a condenser. A data acquisition (DAQ) card with maximum sampling rate of 500 kHz was employed for data collection. Current and voltage signals were measured by a voltage transducer and a Hall Effect current sensor respectively. A high accuracy displacement transducer was installed for the measurement of the actual armature/piston displacement. Data collection and the control of linear motor operation were implemented in LabVIEW. Piston/armature stroke was controlled with a PID controller, in which the amplitude of sine wave voltage that excites the linear motor can be varied automatically to achieve the target stroke. The frequency of voltage can be adjusted manually.

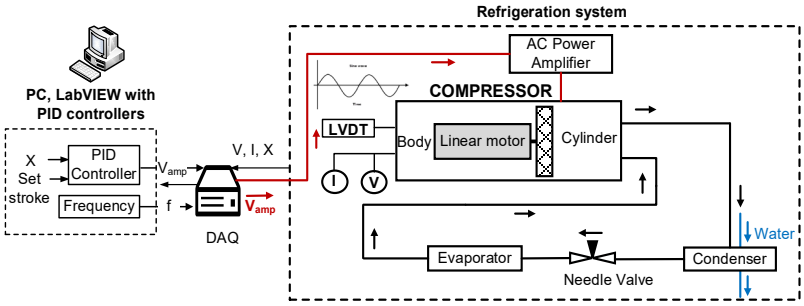

Figure 4. The schematic of the test rig that employed the moving magnet linear motor (LVDT: displacement sensor, V: voltage sensor, I: current transducer).

4. Results and Discussions

4.1. Voltage and Current

Figure 5 shows the current and displacement signals in one cycle from measurements when the linear motor drives the linear compressor with an operating frequency of 34 Hz and a stroke of 11 mm. Both the current and displacement signals are sine waves. The amplitude of current is 1.6 A, and the current lags the displacement by 86 degrees. This results from the combined impact of the equivalent reluctance of gas load, electrical inductance, and capacitance.

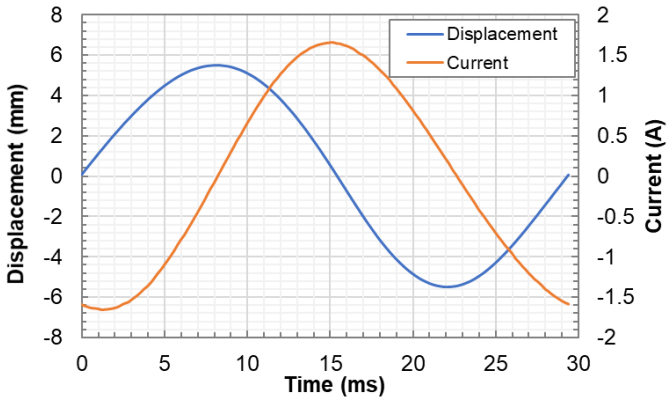

Figure 5. Measured displacement and current in one cycle at a stroke of 11 mm and a frequency of 34 Hz in steady-state.

4.2. THD

Total harmonic distortion (THD) is a measurement index that shows how much voltage or current signals were deviated and distorted from sine waveforms due to harmonics. Higher frequency components exist in a periodical but not purely sinusoidal signal and contribute to the harmonic distortion of the signal. The mathematical definition of THD is shown as follows:

$$\mathrm{THD} = \frac{\sqrt{\sum_{n=2}^{\infty} V_n^2}}{V_1} \tag{4}$$

where V_1 is root mean square (RMS) displacement of the fundamental frequency, and V_n is the RMS displacement of the high order harmonic components. Fast Fourier Transform (FFT) analysis was used to determine the amplitude of each harmonic term. The first six harmonic terms were considered in this study. Lower THD in power systems, suggests less heat generation, smaller peak currents, less motor loss, and lower electromagnetic emissions [26]. Figure 6 shows the THDs of voltage signals at strokes of 9–12 mm for the linear motor that drives the linear compressor. The THD is 1.9% at a stroke of 13 mm. The recommended range of voltage harmonics are within 3% for any single harmonic and 5% for THD [27], which shows that the THDs of voltage of the moving magnet linear motor is within the acceptable range. Generally higher strokes have higher THD. Possible reason for this is that the linear motor is close to saturation with higher strokes where higher currents are supplied.

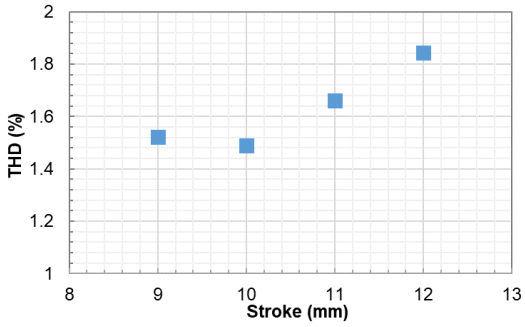

Figure 6. The THDs of measured voltages versus stroke.

4.3. Flux Density

Figure 7 shows the flux density distribution when a sinusoidal RMS 1.2 A current was supplied to drive a motion of a stroke of 10 mm. As can be seen from Figure 7a,b, the magnetic flux density in three cores is similar while the flux density in the other core is much smaller.

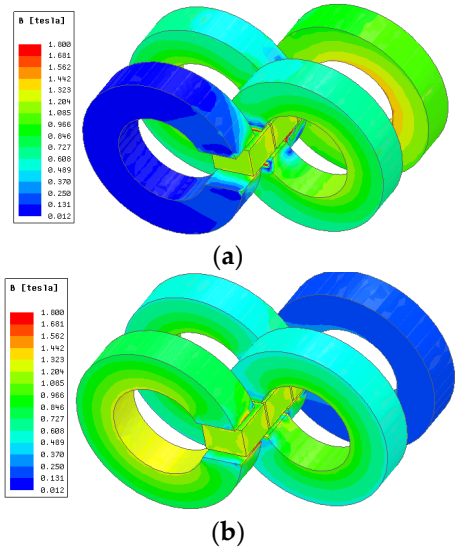

Figure 7. The distribution of magnetic flux density at a stroke of 11 mm and with a sinusoidal RMS 1.2 A current supply (**a**) at displacement of 5.5 mm (**b**) at displacement of 0 mm.

As the armature moves from 0 mm to 5.5 mm, instantaneous current varies from −1.6 A to 0 A, the core of the smallest flux density changes from the one at the most negative side to the most positive side (the positive direction pointing out of the page). Magnetic field in one core is created by electrified windings and permanent magnets. With the variation of permanent position, the air reluctance between each magnet and core changes and the magnetic flux density induced by permanent magnets changes accordingly. As shown in Figure 7, the core at most negative side is the farthest from magnets so that the large magnetic reluctance of air results in the very small flux density in that core.

4.4. Transient Motor Force

Comparison of transient motor (shaft) force between the results from the FEA model and static measurements are shown in Figure 8. The AC current and the motion of magnets were described with harmonic terms that were determined using FFT analysis and were defined in the FEA model. To verify the simulation results, interpolations were made with the Force-Current-Displacement 3-D map from the static motor force measurements [19]. It can be seen that the simulated shaft force from the FEA model is consistent with that of 3-D map interpolation. The motor force varies sinusoidally in one cycle with a peak and a trough at 0.9 ms and 14.1 ms, as shown in Figure 7a, which corresponds to displacement of 0.9 mm and 1.0 mm, respectively. The amplitude of shaft force is 35 N at a stroke of 9 mm and 51 N at a stroke of 11 mm as shown in Figure 8a,b. The maximum error between the motor force calculated from the FEA model and interpolation from the static force measurements is 6% and 9% respectively at peak values.

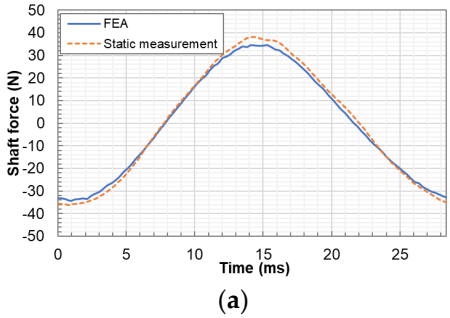

Figure 8. *Cont.*

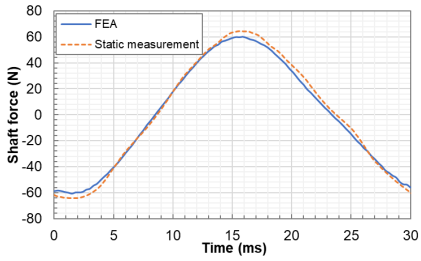

(**b**)

Figure 8. Transient motor force in one cycle from the FEA model and 3-D map interpolation: (**a**) a stroke of 9 mm (**b**) a stroke of 11 mm for the moving magnet linear motor.

4.5. Motor Efficiency

Some of the input power into the linear motor that would ideally be converted into shaft power is lost in the core. The specific total loss against peak magnetic polarization for the core material was tested and provided by the manufacturer. The specific core loss curve (B-H curve) was defined in the simulation environment, and the core losses are calculated for a specific frequency of 50 Hz. The Steinmetz model is often used to estimate iron loss. The total core loss includes eddy current loss and hysteresis loss [28]. It can be expressed as follows:

$$P_{\text{core}} = P_{\text{h}} + P_{\text{e}} = K_{\text{h}} f B^{\alpha} + K_{\text{e}} f^2 B^2 \tag{5}$$

where K_{h}, K_{e} and α are hysteresis and eddy loss coefficients respectively, which are coefficients that depend on lamination, material thickness, conductivity and other factors; B denotes the amplitude of the flux density, and f represents the electrical frequency.

Additional eddy current loss exists in the permanent magnets and windings. The resistive losses of induced eddy currents inside the linear motor can be expressed as follows:

$$P_{ae} = \frac{1}{\sigma} \int J^2 \cdot dV \tag{6}$$

where V is the volume of the body, and J is density of the eddy current.

Based on the FEA model, core loss and additional eddy current loss of coils and magnets in one cycle were calculated as shown in Figure 9. It can be seen that two peak values of core loss and eddy current loss appear in one cycle. It also can be found that the times at which the core loss and eddy current loss reach maximum are close. To calculate the average core loss and additional current loss in one cycle, instantaneous loss was integrated over time and the value was then divided by the period. The average core loss is 0.22 W and the average additional eddy current loss is 0.05 W at a stroke of 12 mm.

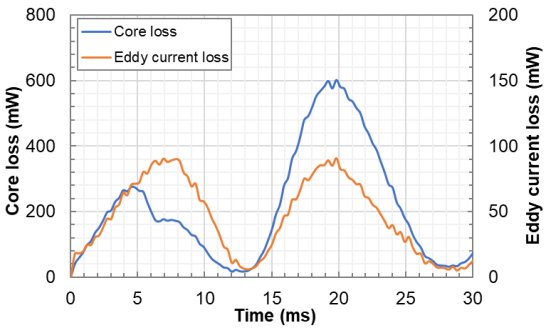

Figure 9. Core loss and additional eddy current loss of coils and magnets in one cycle from the FEA model with a stroke of 12 mm.

Motor efficiency can be calculated as follows:

$$\eta = \frac{P_s}{P_i} = \frac{\int F dv}{P_i} \tag{7}$$

where P_s and P_i are shaft power and input power, F denotes shaft force, and v represents velocity of motion.

Motor efficiency and CoP (coefficient of performance) of the refrigeration system at various strokes are shown in Figure 10. With the increase of stroke, the motor efficiency and CoP show a decreasing trend. When the stroke varies from 9 mm to 12 mm, the motor efficiency decreases from 0.88 to 0.83, and the CoP decreases from 3.7 to 3.5 with a fixed pressure ratio of 2.0. The excitation current increases with stroke leading to higher copper loss, and saturation occurs with the increase of current. It can also be expected that when the heat load is low, lower stroke is only needed so that the motor efficiency is higher than at full capacity. Since the linear motor does not need magnetizing current, there will be no on-off cycling losses. Higher heat load will require higher stroke. Given the fact that the majority of time for refrigerator operation is part load, the seasonal CoP (annual efficiency) could be significantly higher.

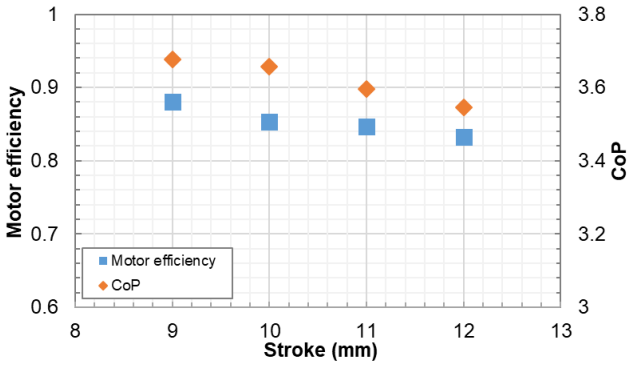

Figure 10. Motor efficiency and CoP versus stroke with a fixed pressure ratio of 2.0 for the moving magnet linear motor/compressor.

4.6. Motor Losses

Copper losses P_{cu} can be easily calculated from the ohmic losses as follows:

$$P_{cu} = I^2 \cdot R \tag{8}$$

where I is the RMS value of current, and R is the total resistance of windings.

The pie charts in Figure 11a,b show the shaft power and losses breakdown of the moving magnet linear motor at a stroke of 9 mm and 11 mm respectively. At a stroke of 11 mm, shaft power accounts for 85% of the input power, the copper loss percentage is 13.5%, while the sum of the rest losses is 1.81%. The majority of loss occurs at windings which transfers into heat dissipated into ambient. It can be seen that the increase of the proportion of copper loss is the main reason for the motor efficiency decrease.

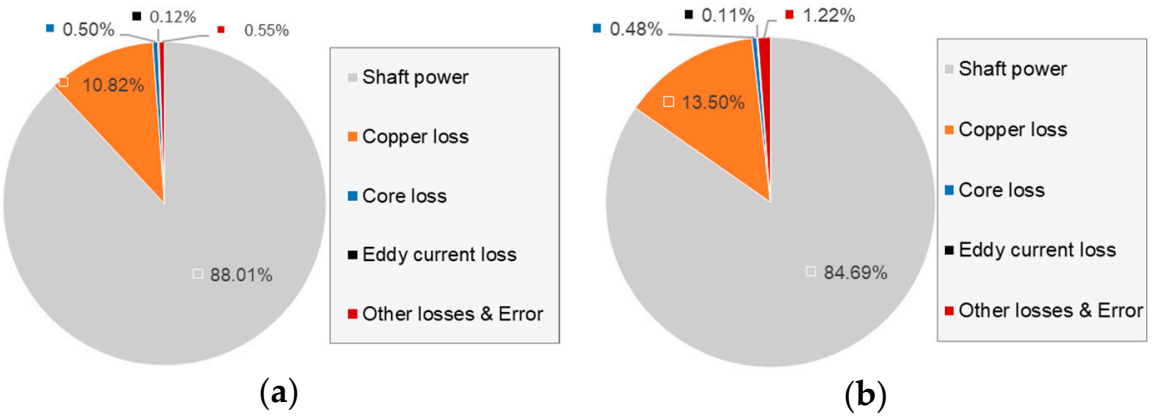

Figure 11. Shaft power and losses for the moving magnet linear motor with a fixed pressure ratio of 2.0 (**a**) a stroke of 9 mm and (**b**) a stroke of 11 mm.

5. Comparisons with Moving Coil Linear Motor

Comparisons were made between the moving magnet design and moving coil linear motor presented in [29] similar to the configuration in Figure 1a as shown in Table 1. The moving mass of the moving coil linear motor is only half of the moving magnet linear motor. A low mover mass suggests high frequency oscillation conditions. To make fair comparisons between the two motors, performance of the motors with the same input power of 40 W and sine waveform driving voltage are listed in the table. The THDs of the two motors are similar. The proportions of copper loss for the moving magnet and moving coil linear motor are 14% and 18% respectively. Note that the motor efficiency of the moving coil linear motor reported in [29] was calculated with consideration of copper loss only. The actual motor efficiency should be smaller than the reported value with other losses taken into account. The moving magnet design shows a higher motor efficiency than the moving coil design.

Table 1. Comparisons between the moving magnet design and the moving coil design [29].

Parameter	Moving Magnet	Moving Coil
Moving mass (kg)	0.66	0.313
Resistance of motor coil (Ω)	3.5	2.62
Stroke (mm)	11.5	8
THD of current (%)	>50	5.2
Copper loss (W)	5.6	7.1
Motor efficiency (%)	84	82 (only considered copper loss)
Motor constant (N/A)	31	28.5
CoP	3.56	3.22

Dang et al. optimized the parameters of a moving coil motor for linear compressor. The manufactured linear compressor was tested and a maximum motor efficiency of 79.48% was reported [30]. It was also reported that the mean motor efficiency for some typical compressors developed for space Stirling-type pulse tube cryocoolers ranges between 74.2% and 83.6% [31]. Compared with moving magnet motors, moving coil designs usually need larger permanent magnets. Moreover, for the effective current transmission from external supply system to the moving coils, required components increase the cost and complexity. Moving magnets outperform moving coil motors for the application into larger compressors as motor efficiency and moving mass becomes more important. To achieve high motor efficiency, copper loss in particular needs to be decreased. One approach is to use coils of larger diameter, thus enabling smaller resistance. The moving mass and resonant frequency of a moving magnet were hardly affected, however, increasing the size of coils results in larger moving mass. Larger moving mass is undesirable for the design of a linear motor, especially when high frequency operation is fancied.

6. Comparisons with Other Moving Magnet Linear Motors

The most widely used tubular design of moving magnet linear motor is shown in Figure 1c. The tubular moving magnet linear motor is composed of an inner stator, an outer stator with coils placed inside, and a moving magnet. LG Electronics who licensed the technology from Sunpower stated that the motor efficiency exceeds 90%, and the LG linear compressor using the tubular moving magnet linear motor is 20–30% more efficient than the conventional compressors [32]. Due to its radial magnetic field, both the laminations of the inner and outer stators should be stacked radially to reduce core loss, which brings manufacturing challenges. The motor characteristics have not been reported in details. To align the piston within the cylinder, the LG linear compressor adopted the tubular moving magnet design and large amounts of coil springs. The overall design appears to be bulky. Wang et al. [33] designed a tubular low-stroke moving magnet linear motor for linear compressor with quasi-Halbach magnetized sintered NdFeB magnets. Maximum motor efficiency of 93% was reported when operated at a stroke of 10 mm at 44.5 Hz, and the motor efficiency decreased to 89% with frequency increased to 46 Hz. However, part load results have not been reported that could be compared to the present rectangular design. A moving magnet design was also proposed by Bijanzad et al. [34,35], who demonstrated that the motor efficiency approached 89% when operated under low load condition using nitrogen as working fluid. However, motor efficiency decreased from 0.79 to 0.7 with input power increasing from 30 to 50 W using R600 as working fluid.

The present moving magnet design provides fair motor efficiency over a wide range of strokes, particularly at part load. The magnet assembly in particular is very simple and robust, but nonetheless, the magnet utilisation is good, the moving mass is low, and high efficiencies are readily attained. The motor shown in Figure 2 has three magnets and four cores but other combinations are possible as long as the number of cores is one greater than the number of magnets.

7. Conclusions

In this paper, a novel moving magnet linear motor for refrigeration compressor was analysed. A transient FEA model was built to simulate the characteristics of the linear motor. Key findings are listed as below:

(1) The transient shaft force varies almost sinusoidally in one cycle, and the shaft force peaks at zero displacement. Close agreements are shown between the transient shaft force from the FEA model and the interpolation results from the static shaft force.
(2) The THDs of voltage were below 2%, which indicates the harmonic deviation is within the acceptable range.
(3) Copper loss of the windings is the major loss of the linear motor, which occupies about 90% of the total loss.
(4) From the comparisons between the moving magnet and moving coil linear motors, the moving magnet type is suggested for scaling up in terms of motor efficiency and superior heat dissipation for coils.
(5) Compared with other moving magnet designs, the present linear motor provides fair motor efficiency with simple structure and low manufacturing difficulties. Part load efficiency is particularly high.

Author Contributions: Conceptualization, K.L.; methodology, H.J., and Z.L.; software, H.J.; validation, H.J. and X.C.; formal analysis, X.C. and H.J.; writing—original draft preparation, X.C.; writing—review and editing, H.J.; supervision, K.L. All authors have read and agreed to the published version of the manuscript.

Funding: This research received no external funding.

Conflicts of Interest: The authors declare no conflict of interest.

References

1. Coulomb, D.; Dupont, J.L.; Pichard, A. 29th Informatory note on refrigeration technologies. In *The Role of Refrigeration in the Global Economy*; IIR document; IIR (International Institute of Refrigeration): Paris, France, 2015.
2. Wang, J.; Jewell, G.W.; Howe, D. A general framework for the analysis and design of tubular linear permanent magnet machines. *IEEE Trans. Magn.* **1999**, *35*, 1986–2000. [CrossRef]
3. Zhang, Y.; Lu, Q.; Yu, M.; Ye, Y. A novel transverse-flux moving-magnet linear oscillatory actuator. *IEEE Trans. Magn.* **2012**, *48*, 1856–1862. [CrossRef]
4. Boldea, I.; Nasar, S.A. Linear electric actuators and generators. *IEEE Trans. Energy Convers.* **1999**, *14*, 712–717. [CrossRef]
5. Wang, J.B.; Howe, D.; Lin, Z.Y. Comparative studies on linear motor topologies for reciprocating vapor compressors. In Proceedings of the IEEE International Electric Machines & Drives Conference, Antalya, Turkey, 3–5 May 2007; pp. 364–369.
6. Lee, H.K.; Park, K.B.; Park, J.S.; Hong, E.P. Linear Motor and Linear Compressor Using the Same. U.S. Patent US2007152516, 25 August 2010.
7. Beers, D.; Barito, T.H.; Gregory, W. Linear Compressor. U.S. Patent US20150226200, 13 August 2015.
8. Song, G.Y. Spring supporting structure of linear compressor. U.S. Patent US6435842B2, 20 August 2002.
9. Noboru, K.; Hiroaki, S.; Kensaku, K. Linear oscillatory actuator. U.S. Patent US8373315B2, 12 February 2013.
10. Jiao, Z.; Wang, T.; Yan, L. Design of a tubular linear oscillating motor with a novel compound halbach magnet array. *IEEE/ASME Trans. Mech.* **2017**, *22*, 498–508. [CrossRef]
11. Zhu, Z.Q.; Chen, X. Analysis of an e-core interior permanent magnet linear oscillating actuator. *IEEE Trans. Magn.* **2009**, *45*, 4384–4387. [CrossRef]
12. Wang, J.; Howe, D.; Lin, J. Development of transverse flux linear motor with permanent-magnet excitation for direct drive applications. *IEEE Trans. Magn.* **2005**, *41*, 1936–1939.
13. Liang, K.; Stone, R.; Hancock, W.; Dadd, M.; Bailey, P. Comparison between a crank-drive reciprocating compressor and a novel oil-free linear compressor. *Int. J. Refrig.* **2014**, *45*, 25–34. [CrossRef]
14. Redlich, R.; Unger, R.; van der Walt, N. Linear compressor: Motor configuration, modulation and system. In Proceedings of the International Compressor Engineering Conference, West Lafayette, IN, USA, 23–26 July 1996; Purdue: West Lafayette, IN, USA, 1996; pp. 1–6.
15. Ibrahim, T.; Wang, J.; Howe, D.; Nor, N.M. Design and optimization of a moving-iron linear permanent magnet motor for reciprocating compressors using finite element analysis. *Int. J. Elect. Comput. Sci.* **2010**, *10*, 1–7.
16. Lee, H.; Wang, S.; Park, K. Iron loss analysis of linear motor for linear compressor. In Proceedings of the International Compressor Engineering Conference, West Lafayette, IN, USA, 12–15 July 2004; Purdue: West Lafayette, IN, USA, 2004; pp. 1–7.
17. Lubin, T.; Mezani, S.; Rezzoug, A. Development of a 2D analytical model for the electromagnetic computation of axial-field magnetic gears. *IEEE Trans. Magn.* **2013**, *49*, 5507–5521. [CrossRef]
18. Tiegna, H.; Amara, Y.; Barakat, G. Overview of analytical models of permanent magnet electrical machines for analysis and design purposes. *Math. Comput. Simul.* **2013**, *90*, 162–177. [CrossRef]
19. Jiang, H.; Liang, K.; Li, Z. Characteristics of a novel moving magnet linear motor for linear compressor. *Mech. Syst. Signal Process.* **2019**, *121*, 828–840. [CrossRef]
20. Chen, N.; Tang, Y.; Wu, Y. Study on static and dynamic characteristics of moving magnet linear compressors. *Cryogenics* **2007**, *47*, 457–467. [CrossRef]
21. Li, X.; Xu, W.; Ye, C.; Boldea, I. Comparative study of transversal-flux permanent-magnetic linear oscillatory machines for compressor. *IEEE Trans. Ind. Electron.* **2018**, *65*, 7437–7446. [CrossRef]
22. Abdalla, I.I.; Ibrahim, T.; Nor, N.B.M. Development and optimization of a moving-magnet tubular linear permanent magnet motor for use in a reciprocating compressor of household refrigerators. *Int. J. Elect. Power Energy Syst.* **2016**, *77*, 263–270. [CrossRef]
23. Ko, K.; Choi, J.; Jang, S.; Choi, J. Analysis of eddy current losses in cylindrical linear oscillatory actuator with Halbach permanent magnet array mover. *J. Appl. Phys.* **2012**, *111*, 07B547. [CrossRef]
24. Abdalla, I.I.; Ibrahim, T.; Nor, N.B.M. Minimization of eddy-current loss in a permanent-magnet tubular linear motor. *Int. J. Adv. Sci. Eng. Inf. Technol.* **2017**, *7*, 964–970. [CrossRef]
25. Ansys Maxwell, ANSYS, Inc. Available online: http://www.ansys.com/ (accessed on 4 August 2019).

26. Associated Power Technologies. *Total Harmonic Distortion and Effects in Electrical Power Systems*; Associated Power Technologies: Lake Forest, IL, USA, 2017.
27. IEEE Std. *IEEE Recommended Practices and Requirements for Harmonic Control in Electrical Power Systems*; IEEE Std: Piscataway Township, NJ, USA, 1993; pp. 519–1992.
28. Smith, A.C.; Edey, K. Influence of manufacturing processes on iron losses. In Proceedings of the 1995 Seventh International Conference on Electrical Machines and Drives, Durham, UK, 11–13 September 1995; pp. 77–81.
29. Li, C.; Li, J.; Tang, L.; Sun, J.; Zou, H.; Cai, J. Effects of the driving voltage waveform on the performance of vapor compression cycle system driven by the moving coil oil-free linear compressor. *Int. J. Refrig.* **2019**, *108*, 200–208. [CrossRef]
30. Dang, H.; Li, J.; Tan, J.; Zhao, Y.; Zha, R.; Zhang, T.; Zhao, B.; Zhao, Y.; Tan, H.; Xue, R. Theoretical modeling and experimental verification of the motor design for a 500 g micro moving-coil linear compressor operating at 90–140 Hz. *Int. J. Refrig.* **2019**, *104*, 502–512. [CrossRef]
31. Dang, H. Development of high performance moving-coil linear compressors for space Stirling-type pulse tube cryocoolers. *Cryogenics* **2015**, *68*, 1–18. [CrossRef]
32. Lee, H.; Song, G.; Park, J.; Hong, E.; Jung, W. Development of the linear compressor for a household refrigerator. In Proceedings of the International Compressor Engineering Conference, West Lafayette, IN, USA, 25–28 July 2000; Purdue: West Lafayette, IN, USA, 2000; pp. 31–38.
33. Wang, J.; Howe, D.; Lin, Z. Design optimization of short-stroke single-phase tubular permanent-magnet motor for refrigeration applications. *IEEE Trans. Ind. Electron.* **2010**, *57*, 327–334. [CrossRef]
34. Bijanzad, A.; Hassan, A.; Lazoglu, I.; Kerpicci, H. Development of a new moving magnet linear compressor. Part A: Design and modeling. *Int. J. Refrig.* **2020**, *113*, 70–79. [CrossRef]
35. Bijanzad, A.; Hassan, A.; Lazoglu, I.; Kerpicci, H. Development of a new moving magnet linear compressor. Part B: Performance analysis. *Int. J. Refrig.* **2020**, *113*, 94–102. [CrossRef]